CXCL10-CXCR3 Enhances the Development of Neutrophil-mediated Fulminant Lung Injury of Viral and Nonviral Origin

Akihiko Ichikawa[1]*, Keiji Kuba[1]*, Masayuki Morita[1], Shinsuke Chida[2], Hiroyuki Tezuka[3,4], Hiromitsu Hara[5], Takehiko Sasaki[2], Toshiaki Ohteki[3,4], V. Marco Ranieri[6], Claudia C. dos Santos[7,8], Yoshihiro Kawaoka[9,10,11], Shizuo Akira[12], Andrew D. Luster[13], Bao Lu[14], Josef M. Penninger[15], Stefan Uhlig[16], Arthur S. Slutsky[7,8], and Yumiko Imai[1]

[1]Department of Biological Informatics and Experimental Therapeutics and [2]Department of Medical Biology, Akita University Graduate School of Medicine, Akita, Japan; [3]Department of Biodefense Research, Medical Research Institute, Tokyo Medical and Dental University, Tokyo, Japan; [4]Core Research for Evolutional Science and Technology (CREST), Japan Science and Technology Agency, Tokyo, Japan; [5]Division of Molecular and Cellular Immunoscience, Department of Biomolecular Sciences, Saga University, Saga, Japan; [6]Dipartimento di Anestesia, Università di Torino, Ospedale S. Giovanni Battista, Torino, Italy; [7]Keenan Research Center at the Li Ka Shing Knowledge Institute of St. Michael's Hospital, Toronto, Canada; [8]Interdepartmental Division of Critical Care Medicine, University of Toronto, Toronto, Canada; [9]Influenza Research Institute, University of Wisconsin-Madison, Madison, Wisconsin; [10]Division of Virology, Department of Microbiology and Immunology and International Research Center for Infectious Diseases, Institute of Medical Science, University of Tokyo, Tokyo, Japan; [11]ERATO Infection-Induced Host Responses Project, Japan Science and Technology Agency, Saitama, Japan; [12]Department of Host Defense, Research Institute for Microbial Diseases, Osaka University, Osaka, Japan; [13]Center for Immunology and Inflammatory Diseases, Division of Rheumatology, Allergy, and Immunology, Massachusetts General Hospital, Charlestown, Massachusetts; [14]Children's Hospital, Harvard Medical School, Boston, Massachusetts; [15]Institute of Molecular Biotechnology in the Austrian Academy of Sciences, Vienna, Austria; and [16]Institute of Pharmacology and Toxicology, Medical Faculty, RWTH Aachen University, Aachen, Germany

***Rationale*: Patients who developed acute respiratory distress syndrome (ARDS) after infection with severe respiratory viruses (e.g., severe acute respiratory syndrome–coronavirus, H5N1 avian influenza virus), exhibited unusually high levels of CXCL10, which belongs to the non-ELR (glutamic-leucine-arginine) CXC chemokine superfamily. CXCL10 may not be a bystander to the severe virus infection but may directly contribute to the pathogenesis of neutrophil-mediated, excessive pulmonary inflammation.**

***Objectives*: We investigated the contribution of CXCL10 and its receptor CXCR3 axis to the pathogenesis of ARDS with nonviral and viral origins.**

***Methods*: We induced nonviral ARDS by acid aspiration and viral ARDS by intratracheal influenza virus infection in wild-type mice and mice deficient in CXCL10, CXCR3, IFNAR1 (IFN-α/β receptor 1), or TIR domain-containing adaptor inducing IFN-β (TRIF).**

***Measurements and Main Results*: We found that the mice lacking CXCL10 or CXCR3 demonstrated improved severity and survival of nonviral and viral ARDS, whereas mice that lack IFNAR1 did not control the severity of ARDS *in vivo*. The increased levels of CXCL10 in lungs with ARDS originate to a large extent from infiltrated pulmonary neutrophils, which express a unique CXCR3 receptor via TRIF. CXCL10-CXCR3 acts in an autocrine fashion on the oxidative burst and chemotaxis in the inflamed neutrophils, leading to fulminant pulmonary inflammation.**

***Conclusions*: CXCL10-CXCR3 signaling appears to be a critical factor for the exacerbation of the pathology of ARDS. Thus, the CXCL10-CXCR3 axis could represent a prime therapeutic target in the treatment of the acute phase of ARDS of nonviral and viral origins.**

AT A GLANCE COMMENTARY

Scientific Knowledge on the Subject

Non-ELR chemokine CXCL10 and its receptor CXCR3 control neutrophil-mediated severe pulmonary inflammation.

What This Study Adds to the Field

The CXCL10-CXCR3 axis represents a therapeutic target in the treatment of the acute phase of acute respiratory distress syndrome of nonviral and viral origins.

(*Received in original form April 4, 2012; accepted in final form September 23, 2012*)

* Co–first authors

Y.I. and K.K. are supported by Funding Program for Next Generation World-Leading Researchers (NEXT Program, JSPS), grants-in-aid for Specially Promoted Research and for Scientific Research, and the Global COE Program. Y.K. is supported by Center of Education and Research for the Advanced Genome-Based Medicine for Personalized Medicine and the Control of Worldwide Infectious Diseases and by a Grant-in-Aid for Specially Promoted Research and by Japan Initiative for Global Research Network on Infectious Diseases from the Ministry of Education, Culture, Sports, Science, and Technology, by ERATO (Japan Science and Technology Agency), and by Public Health Service research grants from the National Institute of Allergy and Infectious Diseases. J.M.P. is supported by IMBA, the Austrian National Bank and the Austrian Ministry of Science and Education. A.S.S. is supported by the Canadian Institutes of Health Research (CIHR) and the Canada Foundation for Innovation (CFI). S.U. was supported by the SFB542 (TPC16) of the Deutsche Forschungsgemeinschaft (DFG, Bonn, Germany). A.D.L. was supported by NIH grant CA069212.

Author Contributions: Conception and design: Y.I.; analysis and interpretation: Y.I., K.K., A.I., M.M., S.C., H.T., H.H., T.O., T.S., V.M.R., C.C.d.S., Y.K., S.A., A.D.L., B.L.; drafting the manuscript for important intellectual content: Y.I., J.M.P., S.U., A.S.S.

Correspondence and requests for reprints should be addressed to Yumiko Imai, M.D., Ph.D., Department of Biological Informatics and Experimental Therapeutics, Akita University Graduate School of Medicine, Akita 010-8543, Japan. E-mail: imai@med.akita-u.ac.jp

This article has an online supplement, which is accessible from this issue's table of contents at www.atsjournals.org

Am J Respir Crit Care Med Vol 187, Iss. 1, pp 65–77, Jan 1, 2013

Originally Published in Press as DOI: 10.1164/rccm.201203-0508OC on November 9, 2012
Internet address: www.atsjournals.org

Keywords: CXCL10; CXCR3; ARDS

Acute respiratory distress syndrome (ARDS) affects approximately 1 million individuals worldwide each year and has a very high mortality rate (30–50%) (1). Many different pathogenic conditions, including sepsis, gastric acid aspiration, and respiratory virus infections such as the severe acute respiratory syndrome (SARS)-coronavirus, the avian H5N1 virus, and the 2009 pandemic H1N1 virus, can cause ARDS (2). In particular, H5N1 avian influenza viruses have spread throughout Asia, Europe, and Africa, primarily infecting poultry and migratory birds; mortality in humans from this infection has been as high

as 60% (3). The natural history of ARDS is marked by exudative (acute), proliferative (subacute), and fibrotic (late) phases. Many patients die in the acute fulminant phase of ARDS, which is characterized by an extremely severe pulmonary inflammatory response accompanied by massive neutrophil accumulation, increased vascular permeability, and high production of cytokines and chemokines (i.e., IL-6, IL-1β, and IL-8)—a so-called "cytokine storm" (4, 5). To date, no effective drugs targeting the underlying pathophysiology have been proven to improve clinical outcomes in ARDS (1, 2). Because of its high lethality and the threats of emerging respiratory virus infections, it is important to identify novel therapeutic targets for ARDS. Patients infected by SARS coronavirus (6) or H5N1 avian influenza (7) who developed ARDS exhibited unusually high levels of C-X-C motif chemokine 10 (CXCL10), also known as IFN-γ–induced protein 10 kD (IP-10), which binds the CXCR3 receptor, inducing chemotaxis, apoptosis, cell growth, and angiostasis (8, 9, 10). Recent highly pathogenic H5N1 virus isolates appear to be even more potent inducers of CXCL10 compared with their less pathogenic earlier counterparts (11–13), suggesting a possible impact of increased CXCL10 levels on disease severity. However, it was previously believed that higher CXCL10 levels were a sequel to virus infections with increased activation of the JAK/STAT pathway (14), and whether CXCL10 contributed directly to the pathogenesis of severe virus-induced ARDS remained unclear. On the other hand, Mob-1 (the rat homolog of human CXCL10) is increased in nonviral experimental lung injury (e.g., IL-2–induced lung injury in rats) (15, 16), although the precise mechanisms remained unclear.

In the present study, we hypothesized that CXCL10 and its receptor, CXCR3, can actively participate in the pathogenesis of the fulminant phase of viral- and nonviral-induced ARDS. Our data also show that mice deficient in CXCL10 or its receptor CXCR3 have decreased lung injury severity and increased survival in response to viral (influenza virus infection) and nonviral (acid aspiration) lung injury. Although CXCR3 was previously believed not to be present on neutrophils (17), we demonstrated the presence of a unique neutrophil population expressing CXCR3 in the inflamed lungs. Mechanistically, CXCL10-CXCR3 acts in an autocrine fashion on the oxidative burst and chemotaxis in inflamed neutrophils, enhancing fulminant inflammation. Moreover, IFN-β_1 was elevated in lungs of viral and nonviral lung injury. To date, it has been controversial as to whether IFN-α/β can contribute to the pathogenesis of severe respiratory virus infection; IFN-α/β receptor 1 (IFNAR1)-deficient mice have accelerated mortality as a result of H5N1 influenza virus (18) but not SARS-coronavirus infection (19). To examine if IFN-α/β can control the severity of ARDS, we analyzed IFNAR1 knockout (KO) mice using viral and nonviral lung injury models. We found that IFNAR1-deficient mice were not protected from severe lung injury. Thus, the CXCL10-CXCR3 axis may be a prime therapeutic target in the treatment of the acute phase of ARDS of either nonviral or viral origin.

METHODS

Characteristics of Patients with ARDS

The study was approved by the local ethics committee (Turin, Italy). We studied 10 patients with ARDS, aged 68 ± 10 years (range, 49–82), who had underlying diagnosis of sepsis (n = 4), bone marrow (BM) transplant (n = 2), pneumonia (n = 3), and multiple trauma (n = 1), who were ventilated with a V_T of 8 ± 1 ml/kg body weight and a mean positive end-expiratory pressure (PEEP) of 16 ± 4 cm H_2O. Patients who had extrapulmonary diseases requiring mechanical ventilation served as control subjects (n = 4). For bronchoalveolar lavage (BAL), patients were sedated, and bronchoscopically guided lavage (instillation of 300 ml 0.9% NaCl) was performed in the middle lobe. Aliquots (20 ml) were instilled and immediately reaspirated. The lavage fluid was diluted to a final volume of 50 ml and filtered through four layers of gauze to eliminate remaining mucus. Samples were stored in aliquots of 50 μl at −80°C until assayed.

Animals

Male Sprague-Dawley rats were purchased from Charles River Laboratories (Wilmington, MA). *cxcl10* (36), *cxcr3* (37), and *trif* (38) mutant mice have been previously described. *Ifnar1* mutant mice were obtained from B&K Universal (Grimston, UK). Background of *cxcl10* (36), *cxcr3* (37), *trif* (38), and *Ifnar1* mutant mice are C57BL/6. C57BL/6 mice were bred at our animal facility. Only sex- and age-matched C57BL/6 mice were used as controls. Basal lung function and lung structure were comparable among all the mice tested. Mice were housed in accordance with institutional guidelines.

Acid Aspiration–induced Lung Injury Model in Rats

Anesthetized (ketamine hydrochloride: 10 mg/kg/h and xylazine: 2 mg/kg/h) rats (400–450 g) were ventilated with a volume-controlled constant flow inflation ventilator (Voltek Enterprises, Toronto, Canada). A carotid arterial line was used to measure arterial blood pressure (Pd 23; Gould, Inc., Cleveland, OH) and to obtain blood for arterial blood gases (Ciba-Corning Model 248; Bayer, Leverkusen, Germany). Lactated Ringer solution (10 ml/kg/h) was infused intravenously. After intratracheal instillation of HCl (pH = 1.5; 2 ml/kg), rats were ventilated for 3 hours ($F_{I_{O_2}}$, 1.0; PEEP, 2.5 cm H_2O). After 3 hours of ventilation, left lungs were snap frozen in liquid nitrogen for RNA extraction, and right lungs were fixed in 10% buffered formalin for pathological examination. Control rats were sacrificed after surgical preparation without acid instillation. Total PEEP (PEEPt) and Pplateau pressure (Pplat) were measured at the end of expiratory and inspiratory occlusion, respectively. Every 30 minutes, elastance was calculated as (Pplat − PEEPt)/V_T.

Acid Aspiration–induced Acute Lung Injury Model in Mice

We used a previously described mouse acid aspiration–induced ARDS model (similar to the rat model described above) for the CXCL10 blockade study (22, 39). Mice were anesthetized with ketamine (75 mg/kg) and xylazine (20 mg/kg) intraperitoneally, tracheostomized, and ventilated with flexiVent system (SCIREQ Inc., Montreal, Canada). Volume recruitment maneuvers (VRM) were performed to standardize volume history, and measurements were made at baseline. After intratracheal instillation of HCl (pH = 1.5; 2 ml/kg), followed by a VRM, mice were ventilated for 3 hours ($F_{I_{O_2}}$, 1.0; PEEP, 2.5 cm H_2O). Saline-treated groups served as controls. Using flexiVent system with low-frequency forced oscillations (SCIREQ Inc.), we measured airway elastance as well as tissue elastance in mice, in which input impedance of the respiratory system (Zrs) is measured over a frequency range from 0.25 to 20 Hz. A model including an airway compartment comprising a frequency-independent airway inertance and a constant-phase tissue compartment comprising coefficients of tissue elastance can be fitted to Zrs, allowing the partitioning of lung function into components representing the mechanical properties of the airways and lung tissue, as described previously (23). At the end of the experiment, left lungs were assessed for lung wet/dry weight ratios or snap frozen in liquid nitrogen for subsequent biochemical analysis. Right lungs were fixed in 10% buffered formalin for histological examination. In separate experiments, BAL (1 ml of PBS × 3) and differential cell counts were performed. For CXCL10 neutralization with anti-CXCL10 antibodies, C57BL/6 mice received either 50 μg intraperitoneally of anti-mouse CXCL10 (R&D Systems Inc., Minneapolis, MN) or isotype-matched control antibodies 30 minutes before surgical procedures. After acid instillation, mice were randomized to four groups: (*1*) control Ab, saline; (*2*) anti-CXCL10 Ab, saline; (*3*) control Ab, acid; (*4*) anti-CXCL10 Ab, acid. Mice were ventilated for 3 hours and analyzed as described above.

Intratracheal Live Influenza Virus Infection–induced Acute Lung Injury Model in Mice

Mice were anesthetized with intraperitoneal injection of ketamine (75 mg/kg) and xylazine (20 mg/kg). The trachea was exposed by opening the neck skin and blunt dissection. A 24-gauge intravenous catheter was inserted into the trachea. Mice received either the suspension of influenza virus (PR8/H1N1) 66.7 × LD_{50} (1 × 10^4 $TCID_{50}$) or 10 × LD_{50} (1.5 × 10^3 $TCID_{50}$) in 50 μl phosphate-buffered saline (PBS) or same volume of PBS through the intratracheal catheter. Mice were monitored daily and weighed every 24 hours after infection. In separate experiments, respiratory function was analyzed at Days 1, 2, and 5 after infection using the flexiVent system (SCIREQ Inc.). In brief, mice were anesthetized with intraperitoneal injection of ketamine (75 mg/kg) and xylazine (20 mg/kg), tracheostomized, and connected via the endotracheal cannula to a ventilator (FlexiVent; SCIREQ, Inc.). Mice were ventilated at rate of 150 breaths/min at a V_T of 10 ml/kg. We measured airway elastance as well as tissue elastance in mice at 1, 2, and 5 days after infection with influenza virus or mock controls, as described above (23).

H5N1 Avian Influenza Isolate, Virus Inactivation, and Inactivated H5N1–induced Lung Injury in Mice

Inactivated avian influenza virus (A/chicken/Yamaguchi/7/04 [H5N1]) was obtained from the Istituto Zooprofilattico Sperimentale delle Venezie (Padova, Italy). The strain was isolated and characterized according to European guidelines (CEC 92/40). Briefly, the virus was inoculated into 9- to 11-day-old specific pathogen–free embryonated fowl eggs by the allantoic route. Hemagglutinating allantoic fluid was collected from eggs, and the isolated virus was inactivated using β-propiolactone. Virus inactivation was confirmed by reinoculation with two blind passages, and viruses were serotyped to confirm specific influenza H5N1 subtype. For *in vivo* acute lung injury (ALI) experiments (22), control wild-type (WT) and CXCL10 KO mice were surgically prepared and ventilated with a volume-controlled constant flow inflation ventilator (Voltek Enterprises, Toronto, Canada) as described above. Then, inactivated H5N1 virus particles (150 μg RNA) and controls (vehicle) were instilled intratracheally, followed by a VRM (35 cm H_2O, 3 s). Mice were then ventilated for 5 hours ($F_{I_{O_2}}$, 1.0; PEEP, 2.5 cm H_2O). PEEPt and Pplat were measured at the end of expiratory and inspiratory occlusion, respectively. Every 30 minutes, airway elastance was calculated as (Pplat − PEEPt)/V_T.

$TCID_{50}$ and Focus-Forming Unit Assays

For $TCID_{50}$ assay, aliquots of culture supernatants or tissue lysates were 10-fold serially diluted with Dulbecco's modified Eagle medium, applied in quadruplicate to 2 × 10^4 MDCK cells/well of a 96-well plate, and incubated at 37°C for 1 hour. The inoculum was removed, and the cells were washed with PBS and supplied with Dulbecco's modified Eagle medium containing 0.2% bovine serum albumin and trypsin (5 μg/ml). On the third day after infection, the $TCID_{50}$ was determined on the basis of the Karber method. For focus-forming unit assay, an immunofluorescence-based titration assay was conducted as described previously (40). Briefly, MDCK cells were plated on 2 × 10^4 cells/well of a 96-well plate (Asahi Techno Glass). At 24 hours after infection with serially diluted supernatants or tissue lysates containing virus, the cells were fixed with paraformaldehyde in PBS containing 0.1% Triton X-100 and washed with PBS three times. Antibody that reacts with common sequences of avian influenza virus nucleoprotein (NP) and matrix protein 1 (M1) (41) was used as a primary antibody to detect viral antigen (H1N1). Antibody binding to viral proteins was detected with an Alexa Fluor 488-conjugated secondary antibody (Molecular Probes, Carlsbad, CA) diluted 1:300 in PBS containing 0.35% bovine serum albumin.

BM Transplantation

BM transplantation was performed in mice as described (22). In brief, recipient mice were irradiated with 1,200 rads. Bones were flushed with RPMI (Life Technologies, Grand Island, NY) with 10% fetal calf serum (Atlanta Biologicals, Norcross, GA) from both femurs and tibias under sterile conditions. Harvested BM cells (1 × 10^6) in 200 μl of media were delivered intravenously through the tail vein of each recipient mouse. Recipient mice were housed in a barrier facility (individually ventilated cages, high-energy particulate arresting filter–filtered air), under pathogen-free conditions before and after BM transplantation. Recipient chimeras were used for experiments 12 weeks after transplantation.

Preparation of RNA, Microarray Hybridization, and Data Analysis

In an acid-aspiration–induced ALI model in rats, total RNA was isolated from rat lung tissue at 3 hours by using RNeasy Mini kit (Qiagen, Valencia, CA). Pooled RNA was hybridized to Affymetrix (Santa Clara, CA) rat RGUA34 GeneChips in duplicate. The analysis for differential gene expression of the Affymetrix RGU34a chips was performed using R packages from Bioconductor (21). Raw CEL files were normalized with the RMA method from the "Affy" package. In a influenza virus–induced ALI model in mice, total RNA was extracted from lung tissue in mice treated with influenza virus (PR8/H1N1) (influenza [PR8] group) or mock-infected mice (control [PBS] group) at 24 hours after infection and hybridized to Illumina mouse Ref-8 v2.0 GeneChips. The calculation of the log fold-changes and the moderated *t* statistics was accomplished using the Limma package (42). For KEGG pathway enrichment analysis we used DAVID Bioinformatics Resources 6.7 (NIH).

Assessment of Blood Oxygenation

Blood samples were obtained from the left ventricle, and Pa_{O_2} was measured (Ciba-Corning Model 248; Bayer) to assess arterial blood oxygenation as an indicator for respiratory failure.

Pulmonary Edema

Pulmonary edema was assessed by measuring lung wet/dry weight ratio as previously described (22, 39). In brief, the lobe of lung was cleaned and weighed to obtain the wet weight and was then placed in an oven at 75°C for 48 hours for the measurement of dry weight. The ratio of wet weight to dry weight was calculated.

Neutrophil Counts in Lung Lavage Fluid

BAL was performed as described above, and total cell number was counted. For cell type differentiation, BAL smears were stained by the Diff-quick method (Fisher Scientific Inc., Waltham, MA). Neutrophil counts are expressed as the percentage of neutrophils multiplied by the total number of cells in the BAL fluid sample.

Immunohistochemistry and Confocal Fluorescence Microscopy

Lung tissue was fixed in 10% buffered formalin and processed for histologic analysis (hematoxylin and eosin) and immunohistochemistry. For immunohistochemistry of CXCL10, a rabbit anti-mouse CXCL10 polyclonal antibody (R&D Systems Inc.) was used. For immunofluorescence staining for CXCL10 and Ly6-G in lung tissues, approximately 5-μm–thick frozen lung sections were prepared from optimal cutting temperature compound–embedded lung tissues. Tissue sections were stained using goat anti-mouse CXCL10 Ab (R&D Systems, Inc.), anti-goat Alexa488 Ab (Invitrogen, Carlsbad, CA), rat Ly6-G Ab (BD, San Jose, CA), and anti-rat Alexa 568 Ab (Invitrogen). For immunofluorescence staining for CXCR3 and Ly6-G in cells in BAL fluid, BAL smears were stained using biotinylated anti-mouse CXCR3 Ab (eBioscience, San Diego, CA), Alexa488 avidin Ab (Invitrogen), rat Ly6-G Ab (BD), and ant-rat Alexa 568 Ab (Invitrogen). Nuclei were stained with Hoechst33342 (Invitrogen). Images were visualized using an A1Rsi confocal microscope (Nikon, Tokyo, Japan).

Macrophage and Neutrophil Isolation from Lung Tissues

Lung tissue cells were prepared as previously described (22). In brief, lung tissues were excised from mice and finely minced and the tissue

pieces placed in medium containing 20 U/ml collagenase and 1 μg/ml DNase. After incubation, any remaining intact tissue was disrupted by passage through a 40-μm cell strainer. The digested cell suspension was then layered on 50% Ficoll, centrifuged at 400 × *g* for 40 minutes, and the macrophage and neutrophil layers were collected.

Isolation of BM-derived Neutrophils

BM-derived neutrophils isolated from healthy WT mice were used as naive neutrophils (control). Mice were killed, and femurs from both hind legs were removed. The distal tip of each edge was cut off, and BM cells were isolated by flushing the femur with Hanks' balanced salt solution. Cell pellets were resuspended and were then layered on 50% Ficoll, centrifuged at 400 × *g* for 40 minutes, and the neutrophil layers were collected. The identification and purity of isolated bone marrow–derived neutrophils, which were stained with Abs Ly6G and CD11b, were examined by flow cytometric analysis.

Neutrophil Adoptive Transfer

BM neutrophils were isolated from WT and CXCL10 KO mice as described above. Isolated neutrophils (1×10^6) in 100 μl of media were injected intratracheally into CXCL10 KO mice. Thirty minutes after neutrophil transfer, recipient CXCL10 KO mice were subjected to acid aspiration–induced lung injury model as described above.

ELISA and Myeloperoxidase Activity

Frozen lung tissues were homogenized in cell lysis buffer, and supernatants were assayed using specific ELISA kits to detect murine CXCL10 and CXCL2/MIP-2 (R&D Systems, Inc.). Human plasma, lung lavage fluid, and culture supernatant in the human cells were assayed using specific ELISA kits for human CXCL10 and IL-8 (R&D Systems, Inc.). Myeloperoxidase (MPO) activity was assayed as reported previously (22). Briefly, lung tissues were homogenized and sonicated in 50 mmol/L potassium phosphate buffer containing hexadecyltrimethylammonium bromide and ethylenediaminetetraacetic acid. After centrifugation, the supernatant was incubated with potassium phosphate buffer containing the substrate, H_2O_2 and *o*-dianisidine dihydrochloride (Sigma Aldrich, St. Louis, MO). The enzymatic activity was determined spectrometrically, and values represent the change in OD/min per gram tissue weight.

Quantitative Real-Time Polymerase Chain Reaction

The measurement of influenza virus NP or cellular RNA was performed by real-time polymerase chain reaction (PCR) analysis with a protocol described. Briefly, RNA was extracted from cells using the RNeasy Mini Kit (Qiagen). First-strand cDNA was synthesized from the DNA-free RNA, using Takara reverse-transcription reagents. Samples of first-strand cDNA were subjected to real-time PCR quantification (Thermal Cycler; Takara, Tokyo, Japan), using forward and reverse primers for the indicated RNA with glyceraldehyde 3-phosphate dehydrogenase or 18S as an invariant control. Relative amounts of mRNA were calculated by using the comparative threshold cycle (C_T) method.

Flow Cytometric Analysis

To examine CXCR3 expression, cells in BAL fluid or BM–derived naive neutrophils were stained with antibodies to CD11b, Ly6G, and CXCR3 (R&D Systems, Inc.), and CXCR3 levels in $CD11b^+Ly6G^+$ cells were analyzed by FACSCalibur (BD). Data were analyzed by FlowJo software (Tree Star, Ashland, OR). Isotype controls were used for all the samples.

Oxidative Burst

Superoxide production was measured using an isoluminol assay in 96-well plates (Greiner Bio-One, Monroe, NC) according to the manufacture's instruction. Cells in KRH (4×10^5) were incubated with 56 μM isoluminol (Tokyo Kasei Kogyo, Tokyo, Japan) and 4.4 U/ml horseradish peroxidase (Sigma) for 10 minutes at 37°C. *N*-Formyl-methionyl-leucyl-phenylalanine (fMLP) (10 μM) (or 40 nM phorbol myristate acetate) was then added to the reaction mixture via the injection port of the SpectraMax L Microplate Reader (Molecular Devices, Sunnyvale, CA), and the light emission was recorded at fixed time intervals.

Chemotaxis Assay

BM neutrophils were isolated from WT mice as described above and were infected with influenza virus (PR8/H1N1) (MOI = 3) or mock for 3 hours. Chemotaxis of the neutrophils toward CXCL2 was assayed using CytoSelect 96-well cell migration assay kit according to the manufacture's assay protocol (Cell Biolabs, San Diego, CA). Briefly, influenza virus- or mock-treated neutrophils were allowed to migrate toward CXCL2 (30 ng/ml) for 1 hour in the presence or absence of CXCL10 (10 ng/ml). Migratory cells were quantified by CyQuant GR Dye.

Statistical Analyses

All data are shown as mean ± SEM. Measurements at single time points were analyzed by unpaired *t* test or analysis of variance with two-tailed *t* tests. Time courses were analyzed by repeated measurements (mixed model) analysis of variance with Bonferroni post *t* tests. Log-rank tests were performed on Kaplan-Meier survival curves. All statistical tests were calculated using GraphPad Prism 5.00 program. *P* less than 0.05 was considered to indicate statistical significance.

RESULTS

Increased CXCL10 in Nonviral Lung Injury

To examine the gene expression profile in nonviral lung injury, we performed a microarray analysis using an acid aspiration–induced lung injury model in rats that recapitulates the acute phase of human ARDS (20). Intratracheal instillation of hydrochloric acid produced an increase in pulmonary elastance that represents changes in pressure achieved per unit changes in volume (Figure 1a) and decreased arterial partial pressure of oxygen (Pa_{O_2}) at 3 hours (Figure 1b). Pa_{CO_2} and mean arterial blood pressure remained relatively constant (*see* Figures E1a and E1b in the online supplement). Histological analysis revealed inflammatory cell infiltration, alveolar hemorrhage, and hyaline membrane formation in acid-treated lungs at 3 hours (Figure 1c). The number of neutrophils in lung lavage fluid was markedly elevated in the acid-treated animals at 3 hours (Figure 1d). Total RNA was extracted from lung tissue in rats treated with acid (acid group) or rats without acid instillation (control group) and hybridized to Affymetrix rat RGUA34 GeneChips. Quantile normalization and differential expression was determined using R (Statistical Package for Microarray Analysis) in the Bioconductor package (21). A total of 625 genes were significantly changed after acid aspiration for 3 hours. Figure E1c summarizes the genes that were up-regulated more than fivefold by acid aspiration–induced lung injury. CXCL10 was the most strongly up-regulated gene. Other cytokines/chemokines, including IL-6, CXCL1 (KC), and CXCL2 (MIP-2), were also highly up-regulated in acid-treated lungs. Functional enrichment analysis identified cytokine–cytokine receptor interaction and cytokine signaling as the top KEGG pathways overrepresented among differentially expressed genes after acid aspiration (Figure 1e). Next, using a mouse model of acid aspiration–induced lung injury (22), we confirmed the up-regulation of CXCL10 mRNA (Figure 1f, *upper panel*) and protein (Figure 1f, *lower panel*) in lungs by quantitative real-time PCR and ELISA, respectively. Acid aspiration resulted in rapid impairment of lung function in WT mice (Figures 2a and Figure 3a) and histological changes with hemorrhage, inflammatory cell infiltration, and hyaline membrane formation (Figure 3b). In addition, the mRNA for CXCL2 and IFN-β_1 were up-regulated in acid-treated lungs (Figure 1g). Next, we determined whether these findings were relevant to

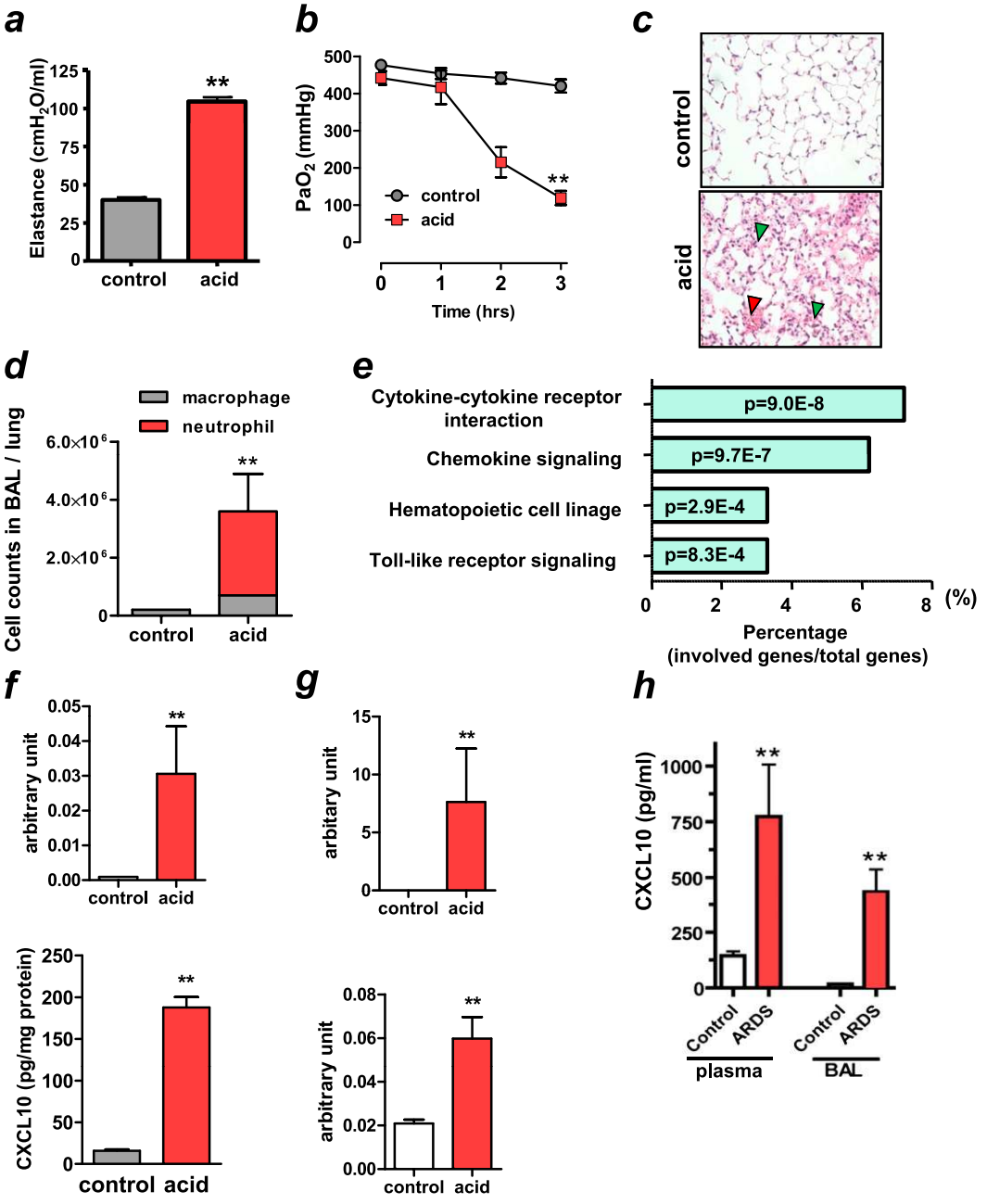

Figure 1. Elevated CXCL10 expression in nonviral lung injury/acute respiratory distress syndrome (ARDS) in animals and patients. (*a–e*) After intratracheal instillation of saline (control) or hydrochloric acid (acid) to rats, animals were ventilated for 3 hours. (*a*) Lung elastance in control and acid treatment at 3 hours. n = 6 each group. $^{**}P < 0.01$ compared with control rats. (*b*) Changes in Pa_{O_2} after saline or acid aspiration. n = 6 each group. $^{**}P < 0.01$ for the whole time course comparing to controls. (*c*) Lung histopathology in control and acid-treated animals at 3 hours. Note inflammatory cell infiltration (*green arrowheads*) and pulmonary hemorrhage (*red arrowhead*) in acid-treated lungs. Hematoxylin and eosin staining. Original magnifications ×200. (*d*) Cell counts in lung lavage fluid in control and acid treatment at 3 hours. n = 4 for control group; n = 6 for acid-treated group. Neutrophil numbers were higher in acid-treated lungs than in control lungs. $^{**}P < 0.01$ compared with control lungs. (*e*) KEGG pathway enrichment analysis of the up-regulated genes after acid aspiration. The numbers inside the columns represent the *P* value of the analysis. (*f, g*) After intratracheal instillation of saline (control) or hydrochloric acid (acid) to mice, animals were ventilated for 3 hours. (*f*) CXCL10 mRNA (*upper panel*) and protein concentration (*lower panel*) in lungs of control and acid-treated animals at 3 hours. n = 4 for control group; n = 6 for acid-treated group. $^{**}P < 0.01$ compared with control lungs. (*g*) CXCL2 (*upper panel*) and IFN-β_1 (*lower panel*) mRNA expressions in lungs of control and acid-treated animals at 3 hours. n = 4 for control group; n = 6 for acid-treated group. $^{**}P < 0.01$ compared with control lungs. (*h*) CXCL10 levels in plasma (*left bars*) and bronchoalveolar lavage fluid (BAL) (*right bars*) in control subjects (n = 17) and patients with ARDS with nonviral origins (n = 10). $^{**}P < 0.01$ compared with control subjects. Data in *a, b, d, f–h* are presented as mean ± SEM.

patients with nonviral ARDS. Compared with control patients with extrapulmonary diseases, all patients with acute-phase ARDS of nonviral origin had high CXCL10 levels in both plasma and BAL fluid irrespective of ARDS etiology (four patients with sepsis, two with BM transplants, three with pneumonia, and one with multiple trauma) (Figure 1h). These data indicate that CXCL10 is increased in the acute phase of nonviral ARDS.

Increased CXCL10 in Viral Lung Injury

Next, we conducted a microarray analysis in an intratracheal influenza virus infection–induced lung injury model in mice. Mice were infected with influenza virus (PR8/H1N1) intratracheally (1×10^4 $TCID_{50}$ [$66.7 \times LD_{50}$]). After intratracheal infection of influenza virus, all mice died within 8 days (Figure E2a). mRNA of virus NP protein from lungs increased after infection (Figure E2b). At 1, 2, and 5 days after infection with influenza virus or mock controls, we measured tissue elastance (Figure 2a) and airway elastance (Figure E2c) in mice, which represent the mechanical properties of the lung tissue and airways, respectively (23). Pulmonary function becomes impaired over time in this viral infection model (Figure 2a and Figure E2c). Histologically, inflammatory cells were increased on Day 2, and alveolar wall thickening, pulmonary edema, hemorrhage, and inflammatory cell infiltration were found on Day 5 after infection in the virus-infected lungs (Figure 2b). Neutrophil numbers were markedly elevated in the virus-infected lungs on Day 5 (Figure 2c). Thus,

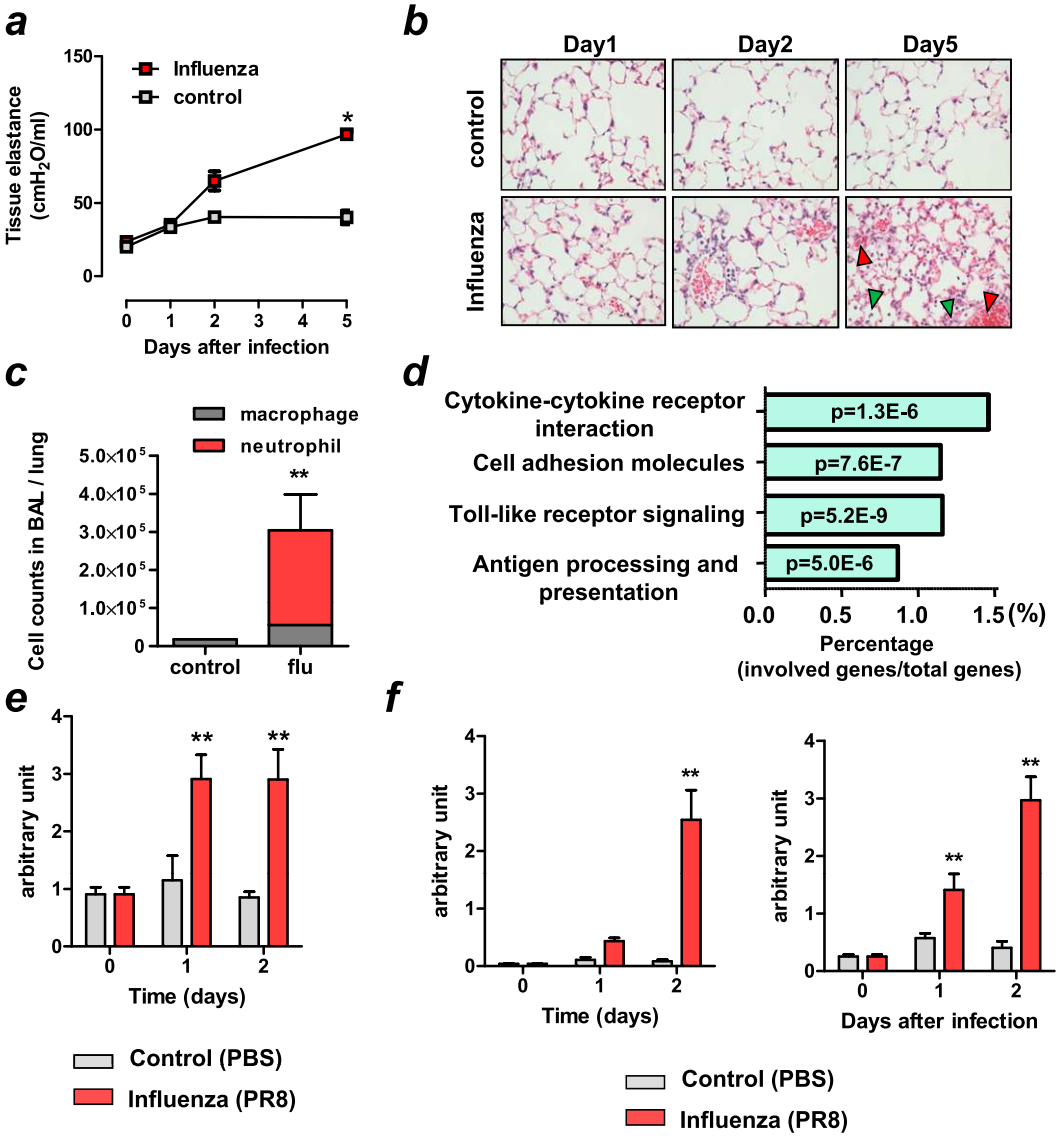

Figure 2. Elevated CXCL10 expression in viral lung injury in mice. (*a–f*) Mice were intratracheally infected with influenza (PR8/H1N1) (1×10^4 $TCID_{50}$ [$66.7 \times LD_{50}$]) virus or mock (control). (*a*) Changes in tissue elastance in mice at 1, 2, and 5 days after infection with influenza virus or mock controls. n = 4 for influenza virus infected group; n = 4 for control group. *$P < 0.05$ for the whole time course comparing to control mice. (*b*) Lung histopathology in mice infected with influenza (PR8/H1N1) virus and control mice. Notably, inflammatory cells were increased on Day 2, and bleeding (*red arrowheads*) and massive inflammatory cell infiltration (*green arrowheads*) were found on Day 5 after infection in the virus-infected lungs. Hematoxylin and eosin staining. Original magnifications ×200. (*c*) Cell counts in lung lavage fluid 5 days after virus-infected or control mice. n = 6 for virus-infected group; n = 4 for control group. Neutrophil numbers were markedly elevated in the virus-infected lungs on Day 5. **$P < 0.01$ compared with control lungs. (*d*) KEGG pathway enrichment analysis of the up-regulated genes after virus treatment. The numbers inside the columns represent the *P* value of the analysis. (*e*) CXCL10 mRNA expression of virus-infected or control lungs at Day 0, 1, and 2. n = 6 for virus-infected group; n = 4 for control group. **$P < 0.01$ compared with control lungs. (*f*) CXCL2 and IFN-β_1 mRNA expressions in lungs of virus-infected or control mice at Day 0, 1, and 2. n = 6 for virus-infected group, n = 4 for control group. **$P < 0.01$ compared with control mice. Data in *a*, *c*, *e*, and *f* are presented as mean ± SEM.

the lung injury model of intratracheal influenza virus closely mimics the acute phase of human ARDS mediated by influenza virus infection. Using this model, total RNA was extracted from lung tissue in mice treated with influenza virus (PR8/H1N1) (influenza [PR8] group) or mock-infected mice (control [PBS] group) 24 hours after infection and hybridized to Illumina mouse Ref-8 v2.0 GeneChips. Figure E2d summarizes results showing the genes that were up-regulated more than fivefold after induction of lung injury, and again CXCL10 was the most strongly up-regulated gene. Pathway enrichment analysis identified enrichment for Toll-like receptor signaling and cytokine–cytokine receptor interaction KEGG pathways among the genes that were found to be up-regulated in viral-induced lung injury (Figure 2d). Up-regulation of CXCL10 mRNA in lungs of virus-treated mice was confirmed by quantitative real-time PCR (Figure 2e). Similar to nonviral lung injury, mRNA expressions of CXCL2 and IFN-β_1 were up-regulated in virus-treated lungs (Figure 2f). These data indicate that CXCL10 is increased in the acute phase of viral lung injury/ARDS.

Mitigation of Nonviral Lung Injury by Blockade of CXCL10-CXCR3

Next, we examined whether deletion of CXCL10 or its receptor, CXCR3, can control the severity of nonviral lung injury in mice. Acid aspiration resulted in rapid impairment of lung function in WT mice as demonstrated by increased pulmonary tissue elastance (Figure 3a), edema formation as assessed by wet to dry weight (Figure E3a), and histological changes with hemorrhage and inflammatory cell infiltration (Figure 3b). In comparison, CXCL10 KO mice exhibited better pulmonary function (Figure 3a) and less edema formation (Figure E3a) with fewer histological changes (Figure 3b). CXCL10 deficiency also resulted in diminished pulmonary neutrophil sequestration as demonstrated by lower neutrophil counts in BAL fluid (Figure 3c). MPO is a hemoprotein that is abundantly expressed in neutrophils and secreted during their activation, and thus MPO activity can be used as an indicator for neutrophil activation (24). Compared with acid-treated WT mice, MPO activity was reduced in lungs of acid-treated

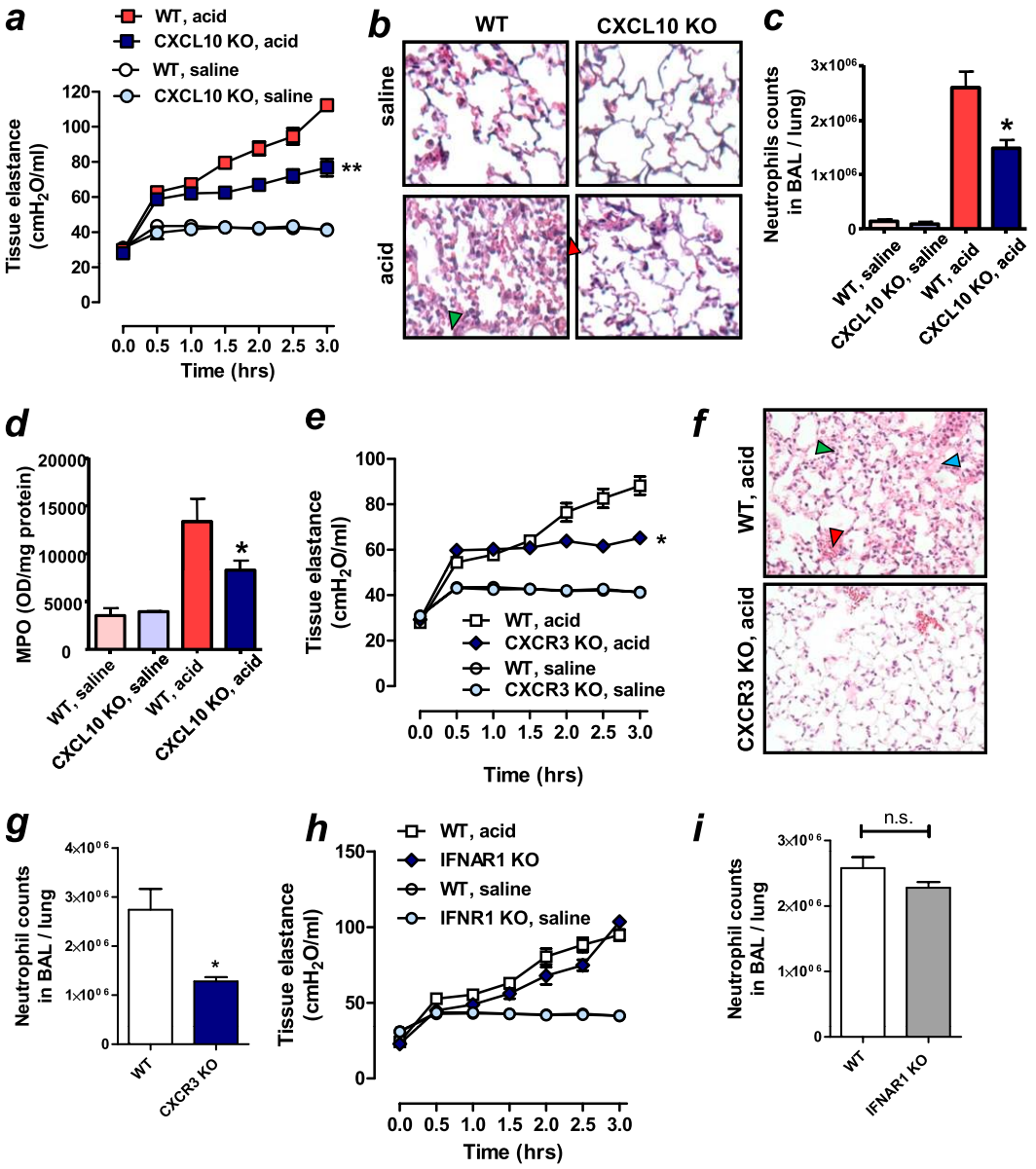

Figure 3. Beneficial effects of CXCL10-CXCR3 blockade in nonviral lung injury in mice. (*a*) Lung tissue elastance after acid or saline treatment in wild-type (WT) and CXCL10 knockout (KO) mice. n = 6–8 for acid-treated groups; n = 6 for saline-treated groups. $^{**}P < 0.01$ for the whole time course comparing acid-treated WT and CXCL10 KO mice. (*b*) Lung histopathology. Lungs were harvested 3 hours after acid treatment. CXCL10 KO mice exhibited reduced inflammatory cell infiltration (*green arrowhead*) and hemorrhage (*red arrowhead*) shown in WT mice . Hematoxylin and eosin (H&E) staining. Original magnifications ×200. (*c*) Neutrophil counts in lung lavage fluid 3 hours after acid or saline treatment in WT and CXCL10 KO mice. n = 6 for acid-treated groups; n = 4 for saline-treated groups.$^{*}P < 0.05$ compared with acid-treated WT mice. (*d*) Myeloperoxidase (MPO) activity in lung tissue 3 hours after acid or saline treatment in WT and CXCL10 KO mice. n = 6 for acid-treated groups; n = 4 for saline-treated groups. $^{*}P < 0.05$ compared with acid-treated WT mice. (*e*) Lung tissue elastance after acid or saline treatment in WT and CXCR3 KO mice. n = 5 each group. $^{*}P < 0.05$ for the whole time course comparing acid-treated WT mice. (*f*) Lung histopathology. Lungs were harvested 3 hours after acid treatment. CXCR3 KO mice exhibited reduced inflammatory cell infiltration (*green arrowhead*), edema (*blue arrowhead*), and hemorrhage (*red arrowhead*) shown in WT mice. H&E staining. Original magnifications ×200. (*g*) Neutrophil counts in lung lavage fluid 3 hours after acid treatment in WT and CXCR3 KO mice. $^{*}P < 0.05$ compared with acid-treated WT mice. (*h*) Lung tissue elastance after acid treatment in WT and IFN-α/β receptor 1 (IFNAR1) KO mice. Changes in lung tissue elastance after acid aspiration were not different between IFNAR1 KO and WT mice. n = 5 each group. (*i*) Neutrophil counts in lung lavage fluid 3 hours after acid treatment in WT and IFNAR1 KO mice. Data in *a*, *c–e*, and *g–i* are presented as mean ± SEM.

CXCL10 KO mice (Figure 3d). Production of CXCL2, a potent neutrophil chemoattractant (Figure E3b) was also reduced in lungs from acid-treated CXCL10 KO mice. Moreover, neutralization of CXCL10 with a specific antibody improved pulmonary function (Figure E3c) and decreased pulmonary edema formation (Figure E3d) and neutrophil infiltration into the lung (Figure E3e). Similar to CXCL10 KO mice, CXCR3 KO mice showed improved lung function (Figure 3e) and histological changes (Figure 3f) in the acid-treated lungs. Neutrophil counts in BAL fluid after acid treatment were less in CXCR3 KO mice compared with WT mice (Figure 3g). Because type I IFNs were also up-regulated in the acid-treated lungs in WT mice (Figure 1h), we next tested whether type I IFNs were involved in the pathogenesis of acid aspiration–induced lung injury using IFNAR1 KO mice. Changes in lung function after acid aspiration were comparable between IFNAR1 KO mice and WT mice (Figure 3h). Neutrophil counts in BAL fluid after acid treatment were not different between CXCR3 KO mice and WT mice (Figure 3i). These data suggest that type I IFNs are unlikely involved in the pathology of acid aspiration–induced lung injury in mice.

Improvement of Viral Lung Injury by Blockade of CXCL10-CXCR3

Next, we determined whether deletion of CXCL10 or CXCR3 could control the severity of influenza virus–induced lung injury in mice. Using a live influenza virus (PR8/H1N1) (Figure 2), we tested whether CXCL10 or CXCR3 deficiency could improve the severity of influenza virus–induced lung injury. Compared with WT mice, CXCL10 KO (Figure 4a) or CXCR3 KO (Figure 4b) mice exhibited improved survival in mice infected with influenza

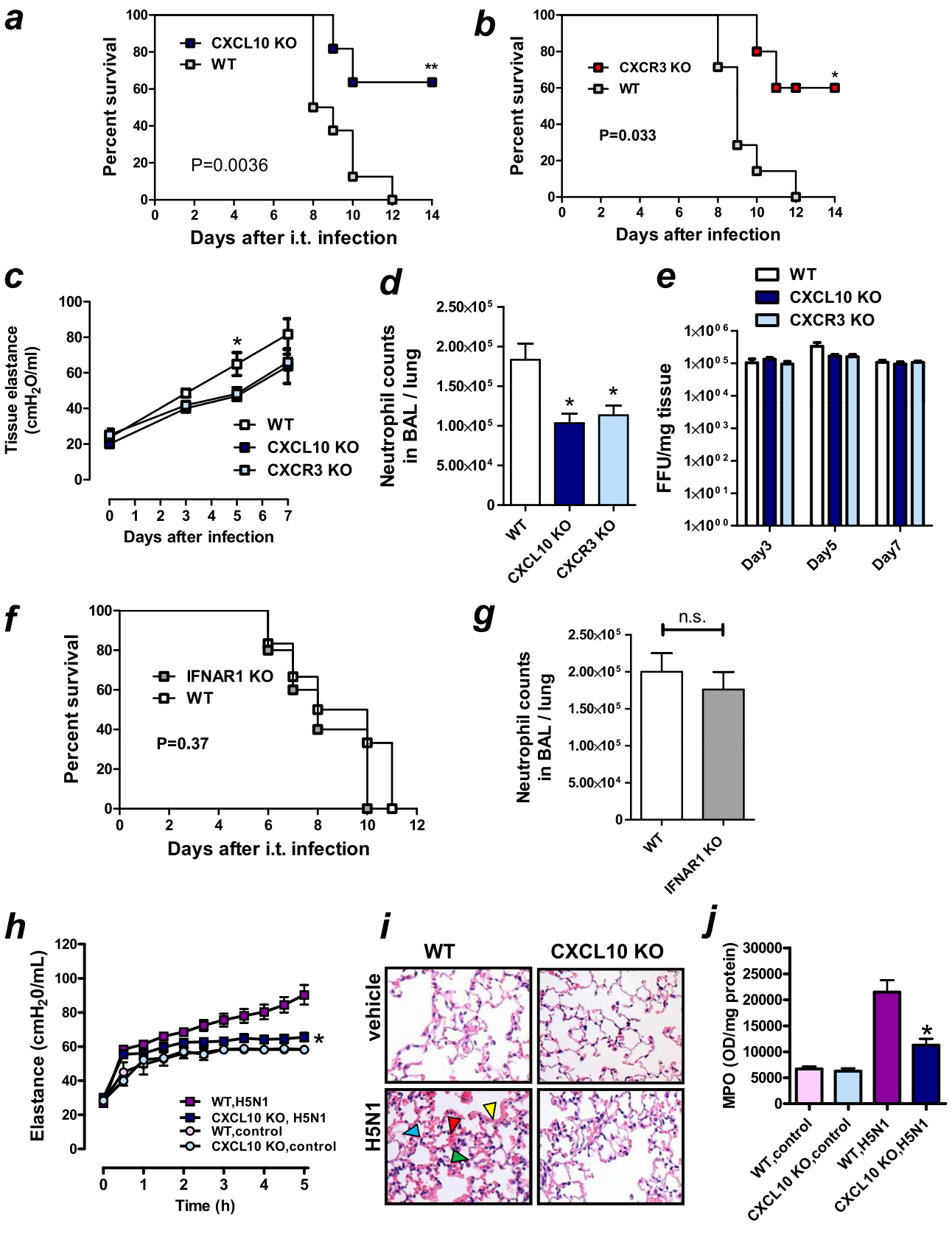
a
Percent survival
CXCL10 KO
WT
P=0.0036
**
Days after i.t. infection
b
Percent survival
CXCR3 KO
WT
P=0.033
*
Days after infection
c
Tissue elastance (cmH2O/ml)
*
WT
CXCL10 KO
CXCR3 KO
Days after infection
d
Neutrophil counts in BAL / lung
*
*
WT
CXCL10 KO
CXCR3 KO
e
WT
CXCL10 KO
CXCR3 KO
FFU/mg tissue
Day3
Day5
Day7
f
Percent survival
IFNAR1 KO
WT
P=0.37
Days after i.t. infection
g
n.s.
Neutrophil counts in BAL / lung
WT
IFNAR1 KO
h
Elastance (cmH2O/mL)
*
WT,H5N1
CXCL10 KO, H5N1
WT,control
CXCL10 KO,control
Time (h)
i
WT
CXCL10 KO
vehicle
H5N1
j
MPO (OD/mg protein)
*
WT,control
CXCL10 KO,control
WT,H5N1
CXCL10 KO,H5N1

Figure 4. Beneficial effects of CXCL10–CXCR3 blockade in viral lung injury in mice. (*a–g*) Wild-type (WT), CXCL10 knockout (KO), CXCR3 KO, and IFN-α/β receptor 1 (IFNAR1) KO mice were intratracheally infected with influenza (PR8/H1N1) virus (1,000 $TCID_{50}$ [$6.7 \times LD_{50}$]) or mock (control). (*a*) Survival of WT or CXCL10 KO mice infected with influenza (PR8/H1N1) virus. n = 7 for each group. $^{**}P < 0.01$ compared with WT mice. (*b*) Survival of WT or CXCR3 KO mice infected with influenza (PR8/H1N1) virus. n = 7 for each group. $^{*}P < 0.05$ compared with WT mice. (*c*) Lung tissue elastance in WT, CXCL10 KO, and CXCR3 KO mice at 0, 3, 5, and 7 days after virus infection. n = 4 for each group. $^{*}P < 0.05$ compared with CXCL10 KO or CXCR3 KO mice. (*d*) Neutrophil counts in lung lavage fluid obtained from WT, CXCL10 KO, and CXCR3 KO mice at 5 days after influenza virus. n = 4 for each group. $^{*}P < 0.05$ compared with WT mice. (*e*) Virus titers assessed by focus forming unit (FFU) assay in lung tissues obtained from WT, CXCL10 KO, and CXCR3 KO mice at 5 days after influenza virus infection. n = 4 for each group. (*f*) Survival of WT and IFNAR1 KO mice infected with influenza (PR8/H1N1) virus. n = 7 for each group. (*g*) Neutrophil counts in lung lavage fluid obtained from WT and IFNAR1 KO mice at 5 days after influenza virus. n = 4 for each group. (*h–j*) After intratracheal bolus instillation of inactivated H5N1 virus particles or control, mice were ventilated for 5 hours. (*h*) Changes in lung elastance in WT and CXCL10 KO mice. n = 6 for each group. $^{*}P < 0.05$ for the whole time course comparing H5N1 virus–treated WT mice. (*i*) Lung histology 5 hours after inactivated H5N1 virus particles or vehicle treatment. CXCL10 KO mice showed reduced inflammatory cell infiltration (*green arrowhead*), hemorrhage (*red arrowhead*), edema (*blue arrowhead*), and hyaline membrane formation (*yellow arrowhead*), shown in inactivated H5N1 virus-treated WT mice. Hematoxylin and eosin staining. Original magnifications ×200. (*j*) Myeloperoxidase (MPO) activity in lung tissue 5 hours after pulmonary administration of vehicle or inactivated H5N1 virus particles. n = 6 for each group. $^{*}P < 0.05$ comparing H5N1-treated WT mice. Data in *c–e, g, h,* and *j* are presented as mean ± SEM.

virus (1.0×10^3 $TCID_{50}$ [$6.7 \times LD_{50}$]). Tissue elastance was also improved in CXCL10 KO and CXCR3 KO 5 days after infection (Figure 4c). Neutrophil counts in BAL fluid at 5 days after infection were significantly less in CXCL10 KO or CXCR3 KO mice than WT mice (Figure 4d). In contrast, virus titers at 3, 5, and 7 days after infection were comparable among WT, CXCL10 KO, and CXCR3 KO mice (Figure 4e). Consistent with acid aspiration–induced nonviral lung injury model, survival (Figure 4f) and neutrophil counts in BAL fluid 5 days after infection (Figure 4g) were not different between IFNAR1 KO and WT mice. These data indicate that deletion of CXCL10 or CXCR3, but not IFNAR1, markedly improved the severity of viral lung injury.

To further determine the impact of CXCL10 deficiency on pulmonary inflammation independent of virus replication, we used an inactivated H5N1 influenza virus–mediated mouse lung injury model, as we previously described (22). A bolus intratracheal instillation of inactivated H5N1 influenza virus caused rapid impairment of lung function (i.e., increased elastance [Figure 4h] and edema formation [Figure E3e]). CXCL10 KO mice treated with this virus showed improved elastance (Figure 4h) and histological signs of lung injury (Figure 4i). In keeping with a protective effect, MPO activity (Figure 4j), CXCL2 levels (Figure E3f), and pulmonary edema formation (Figure E3g) were decreased in CXCL10-deficient mice challenged with H5N1 virus. These data suggest that deletion of CXCL10 or CXCR3 improved the severity of influenza virus–induced lung injury most likely independent of virus replication.

CXCL10 and Its Receptor CXCR3 Expression in Inflamed Neutrophils

We then examined which cell types are responsible for CXCL10-mediated lung injury. We conducted experiments using BM chimeras. Transfer of CXCL10 KO BM into WT mice or transfer of CXCL10 KO BM into CXCL10 KO recipients significantly improved lung functions (Figure E4a) and reduced pulmonary MPO activity (Figure E4b) and CXCL2 levels (Figure E4c) in an acid aspiration–induced lung injury model. Conversely, transfer of WT type BM into CXCL10 KO hosts markedly enhanced the severity of lung injury as compared with mice with CXCL10 mutations in BM cells (Figures E4a–E4c). Of note, there was a significant difference in lung function between transfer of WT BM into CXCL10 KO mice and transfer of CXCL10 KO BM into WT mice. These data indicate that CXCL10 in hematopoietic cells, including macrophages and neutrophils, controls the severity of lung injury.

Next we sought to identify which cell type(s) produce CXCL10 in lungs with lung injury/ARDS. Using immunohistochemistry, we found abundant CXCL10-positive cells in the acid-treated lung at 3 hours (Figure 5a, *right upper panel*) and influenza virus–infected lungs 5 days after infection (Figure 5a, *right lower panel*), most of which appeared to be macrophages and neutrophils. Moreover, CXCL10 mRNA expression was significantly elevated in neutrophils isolated from lungs of mice treated with acid for 3 hours (Figure 5b, *left panel*) or infected with influenza viruses for 5 days (Figure 5b, *right panel*) as a previous study had shown CXCL10 expression from polymorphonuclear neutrophils (25). Macrophages isolated from acid- or virus-treated lungs also expressed CXCL10, but at a lower rate (Figure 5b). These data suggest that CXCL10 was largely produced in fulminant phase of neutrophils but not by naive neutrophils in both nonviral and viral lung injury. Remarkably, other non-ELR motif CXC chemokines CXCL9 and IFN-β were largely produced in macrophages rather than neutrophils in injured lungs (Figure 5c). In contrast, CXCL2 was largely produced by neutrophils in injured lungs (Figure 5c), as previously reported (5).

CXCL10 binds to CXCR3, a G-protein–coupled receptor, which is known to be expressed on activated T lymphocytes, natural killer (NK) cells, and on some epithelial and endothelial cells. CXCR3 was previously believed not to be present on naive neutrophils (17). However, recent studies have shown the expression of CXCR3 on neutrophils from patients with chronic lung disease but not in healthy control subjects (26). Thus, we next tested whether CXCR3 was present on inflamed neutrophils in lungs with fulminant injury. CXCR3 mRNA was significantly up-regulated in neutrophils in lungs obtained from mice treated with acid for 3 hours (Figure 5d, *upper panel*) or influenza virus infection for 5 days (Figure 5d, *lower panel*), whereas it was almost absent in naive neutrophils in lungs obtained from control mice (Figure 5d). Also, CXCR3 protein was mapped to Ly6G-positive neutrophils in BAL cells obtained from influenza virus–infected mice (Figure 5e, *lower panel*), but not BM-derived naive neutrophils (Figure 5e, *upper panel*). Moreover, flow cytometric analysis demonstrated that CXCR3 expression was higher in BAL neutrophils obtained from influenza virus infected–mice than BM-derived naive neutrophils (Figure 5f).

We previously demonstrated that the Toll-like receptor 4 (TLR4)-TRIF axis represents a common pathway responsible for lung injury (22). We therefore investigated whether TRIF is involved in the induction of CXCR3 in inflamed neutrophils. As shown in Figure 5g, CXCR3 expression was induced in inflamed neutrophils isolated from virus-infected WT mice

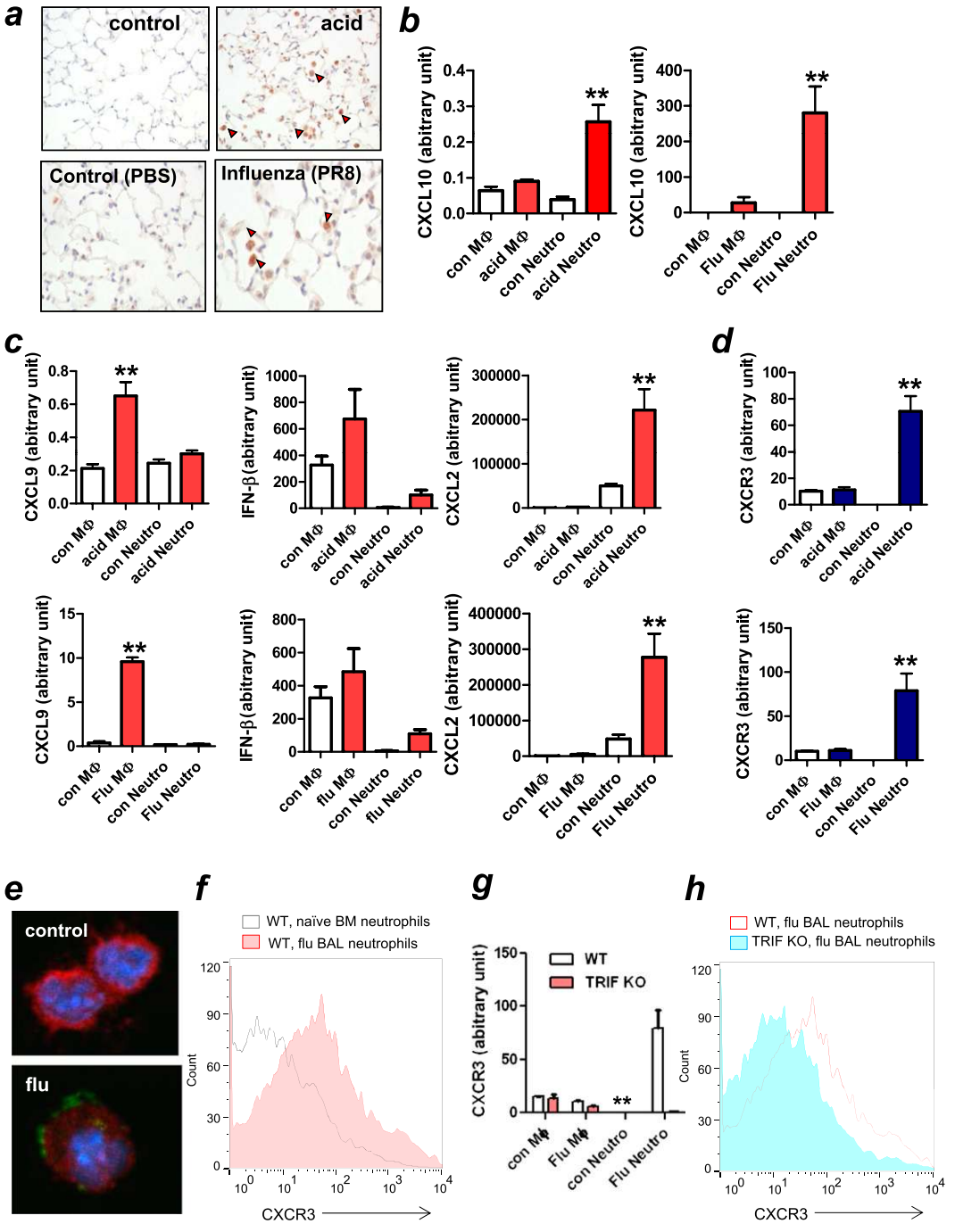

Figure 5. CXCL10 and its receptor CXCR3 expression in inflamed neutrophils. (*a*) Immunohistochemistry of CXCL10 in acid-treated (*upper panels*) or influenza virus–treated lungs (5 d after infection, 1×10^4 $TCID_{50}$) (*lower panels*). *Red arrowheads* mark positive staining of CXCL-10. (*b*) CXCL10 expression in macrophages and neutrophils isolated from acid-treated (*left panel*) or virus-treated (*right panel*) lungs. n = 5 for each group. $^{**}P < 0.01$ compared with control neutrophils. (*c*) Cytokine (CXCL9, IFN-β, and CXCL2) expression in macrophages and neutrophils isolated from acid-treated (*upper panel*) and virus-treated (*lower panel*) lungs. n = 5 for each group. $^{**}P < 0.01$ compared with control lungs. (*d*) CXCR3 expression in macrophages and neutrophils isolated from acid-treated for 3 hours (*upper panel*) and influenza virus–infected for 5 days (*lower panel*) lungs. n = 5 for each group. $^{**}P < 0.01$ compared with control neutrophils. (*e*) Immunohistochemistry of CXCR3 (*green*), Ly6G (*red*), and Hoechst (*blue*) in cells obtained by bronchioalveolar lavage (BAL) from mice infected with influenza virus (PR8/H1N1) for 5 days and bone marrow (BM)-derived naive neutrophils (control). CXCR3 was mapped to Ly6G-positive neutrophils in BAL fluid obtained from virus-infected mice, but not BM-derived naive neutrophils. (*f*) Flow cytometric analysis of CXCR3 expression in $CD11b^+$ $Ly6G^+$ neutrophils of BAL fluid obtained from influenza virus (PR8/H1N1)-infected wild-type (WT) mice for 5 days, or BM-derived neutrophils obtained from healthy mice (naive neutrophils). Representative data from three independent experiments are shown. (*g*) CXCR3 expression in macrophages and neutrophils isolated from mock-treated or virus-treated lungs in WT and TRIF knockout (KO) mice. n = 4 for each group. $^{**}P < 0.01$ compared with TRIF KO mice. (*h*) Flow cytometric analysis of CXCR3 expression in $CD11b^+Ly6G^+$ neutrophils of BAL fluid obtained from influenza virus (PR8/H1N1)-infected WT or TRIF KO mice for 5 days. Representative data from three independent experiments are shown. Data in *b–d* and *g* are presented as mean ± SEM.

but was abolished in neutrophils isolated from virus-infected TRIF KO mice. Furthermore, CXCR3 expression by flow cytometric analysis was less in BAL neutrophils obtained from virus-infected TRIF KO mice than the virus-infected WT mice (Figure 5h). These data suggest that the infiltrated neutrophils in lungs with ARDS, but not noninfiltrated naive neutrophils, express CXCR3 via the TRIF pathway. Our data indicate an induction of CXCL10 originating from neutrophils, and a unique neutrophil population expressing CXCR3, in fulminant lung injury, prompting us to examine a possible autocrine loop of CXCL10 and CXCR3 on neutrophils as described below.

Activation of Oxidative Burst and Chemotaxis in Inflamed Neutrophils by CXCL10-CXCR3

To test whether CXCL10-CXCR3 can activate neutrophils in an autocrine fashion, we examined the effect of CXCL10 on fMLP-induced oxidative burst in neutrophils isolated from acid-treated versus control lungs. We found that treatment with

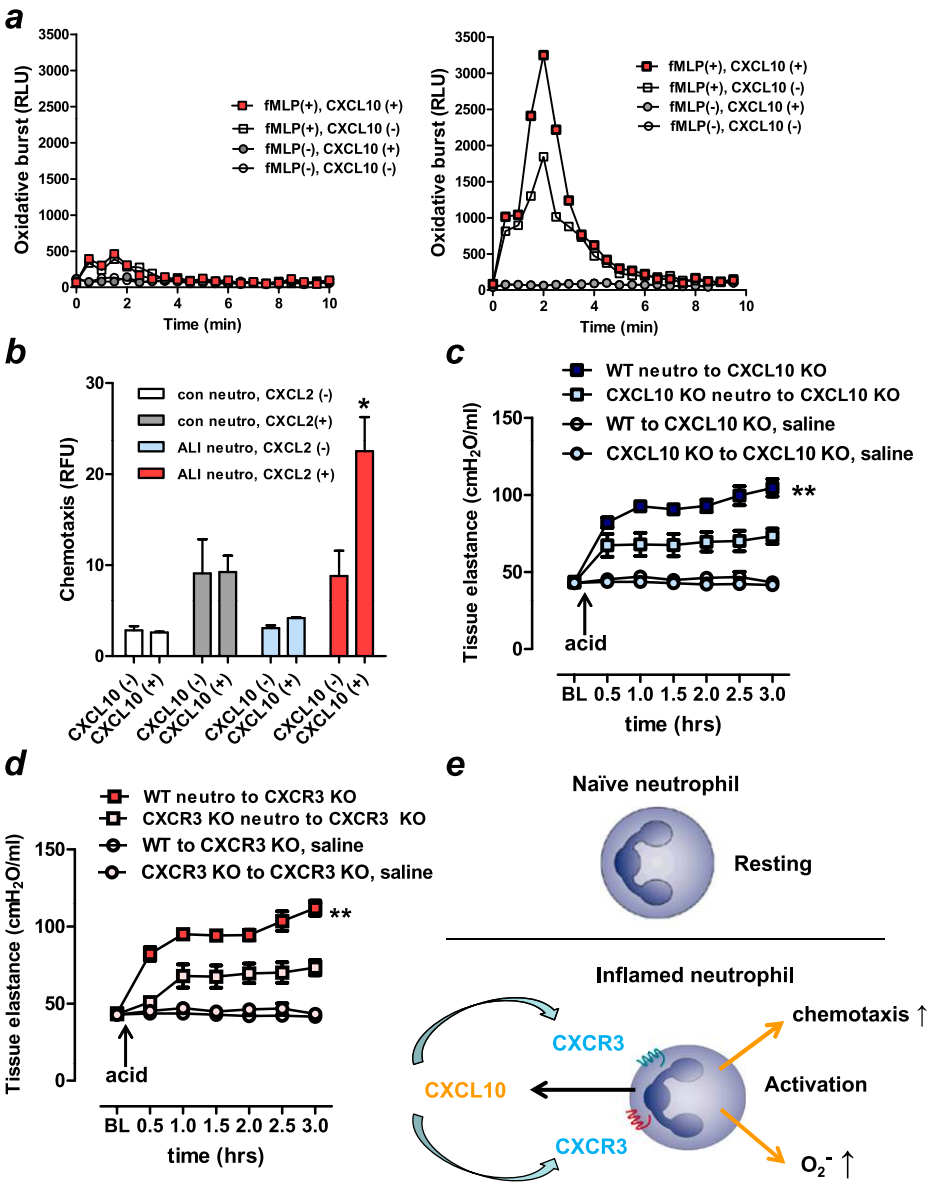

Figure 6. Activation of oxidative burst and chemotaxis in inflamed neutrophils by CXCL10–CXCR3. (*a*) Superoxide generation in naive (*left panel*) and inflamed (*right panel*) neutrophils, isolated from lung tissues obtained from control and acid-treated mice, respectively. CXCL10 enhanced formyl-methionyl-leucyl-phenylalanine (fMLP)-induced superoxide generation in inflamed, but not in naive neutrophils. Three independent experiments were done. (*b*) Chemotactic activity toward CXCL2 in neutrophils isolated from lung tissues obtained from control and acid-treated (lung injury) mice. CXCL10 enhanced the chemotaxis of acid-treated (lung injury), but not naive neutrophils. $*P < 0.05$ compared with acid-treated neutrophils without CXCL2 treatment. (*c*) Neutrophils were isolated from lungs obtained from wild-type (WT) or CXCL10 knockout (KO) mice at 3 hours after acid treatment. Isolated neutrophils (5×10^5) were intratracheally injected into the lungs of the CXCL10 KO mice, and the mice were subjected to an acid aspiration–induced lung injury model for 3 hours. Changes in tissue elastances after acid treatment of CXCL10 KO mice intratracheally transplanted with WT neutrophils (WT neutrophils→CXCL10 KO), and CXCL10 KO mice receiving CXCL10 KO neutrophils (CXCL10 KO neutrophils→CXCL10 KO) were shown. n = 5 for each group. $**P < 0.01$ for the whole time course comparing WT neutrophils→CXCL10 KO and CXCL10 KO neutrophils→CXCL10 KO. (*d*) Neutrophils were isolated from lungs obtained from WT or CXCR3 KO mice at 3 hours after acid treatment. Isolated neutrophils (5×10^5) were intratracheally injected into the lungs of the CXCR3 KO mice, and the mice were subjected to an acid aspiration–induced lung injury model for 3 hours. Changes in tissue elastances after acid treatment of CXCR3 KO mice intratracheally transplanted with WT neutrophils (WT neutrophils→CXCR3 KO), and CXCR3 KO mice receiving CXCR3 KO neutrophils (CXCR3 KO neutrophils→CXCR3 KO) were shown. n = 5 for each group. $**P < 0.01$ for the whole time course comparing WT neutrophils→CXCR3 KO, and CXCR3 KO neutrophils→CXCR3 KO. (*e*) Scheme showing the postulated mechanisms by which CXCL10 is involved in neutrophil-mediated severe pulmonary inflammation. The scheme is based on the functional analysis reported in this paper. *See* DISCUSSION for details. Data in *b–d* are presented as mean ± SEM.

CXCL10 enhanced fMLP-induced superoxide generation in neutrophils isolated from the acid-treated (Figure 6a, *right panel*) but not from control (Figure 6a, *left panel*) lungs. Similar to oxidative burst (Figure 6a), chemotaxis activity toward CXCL2 was enhanced by CXCL10 in neutrophils isolated from the acid-treated but not from control lungs (Figure 6b). Such inflamed neutrophils expressed CXCR3 (Figures 5d–5h). These data suggest that CXCL10 can enhance oxidative burst as well as chemotaxis in inflamed, but not in naive, neutrophils in an autocrine fashion during lung injury.

Finally, to examine whether the CXCL10-CXCR3 axis on neutrophils can control the severity of lung injury *in vivo*, we performed neutrophil adoptive transfer experiment in mice. Neutrophils isolated from WT or CXCL10 KO mice were adoptively transferred into CXCL10 KO mice, and the mice were subjected to an acid aspiration–induced lung injury model. Compared with transfer of CXCL10 KO neutrophils into CXCL10 KO mice, transfer of WT neutrophils into CXCL10 KO mice significantly impaired pulmonary function assessed by pulmonary tissue elastance (Figure 6c) and total respiratory system elastance (Figure E5a). Similarly, after acid aspiration, transfer of WT neutrophils into nontreated CXCR3 KO mice significantly impaired pulmonary function assessed by pulmonary tissue elastance (Figure 6d) and total respiratory system elastance (Figure E5b). These data suggest that CXCL10 and CXCR3 on inflamed neutrophils can participate in the pathogenesis of lung injury *in vivo*.

DISCUSSION

CXCL10 belongs to the non-ELR CXC chemokine superfamily that lacks the normal Glu-Leu-Arg tripeptide sequence adjacent to the CXC motif. Non-ELR CXC chemokines were believed to be chemoattractant for T cells and NK cells but not neutrophils (8–10). CXCL10 was reported to play a role in T-cell or NK-cell–mediated diseases, such as multiple sclerosis (27), asthma (28), allograft rejection (29), and fibrosis (30–32). To our

surprise, the increased levels of CXCL10 in lungs with lung injury originated to a large extent from infiltrated pulmonary neutrophils, which express a unique CXCR3 receptor. In addition, CXCL10-CXCR3 acts in an autocrine fashion on the oxidative burst and chemotaxis in the inflamed neutrophils, leading to fulminant pulmonary inflammation (Figure 6f). Thus, apart from being a possible biomarker, CXCL10 appears to be a critical factor for the exacerbation, but not the initiation, of the inflammatory response and may thus be responsible for the untoward effects of inflammation that cause lung injury.

We previously demonstrated that activation of the TLR4-TRIF pathway by damage-associated molecular patterns (33) derived from dying cells is a common signaling pathway responsible for the pathogenesis of lethal lung injury caused by multiple nonviral (i.e., acid aspiration) and viral (i.e., SARS, H5N1 influenza, anthrax) stimuli (22). Interestingly, CXCL10 is a key chemokine downstream of the TLR4-TRIF pathway and is also produced in lungs stimulated with either TLR2- or TLR4-receptor ligands (34). Here we demonstrate that CXCL10 is critically involved in the pathogenesis of the acute phase of nonviral and viral lung injury/ARDS. Also, we show a neutrophil population expressing CXCR3 receptors via TRIF in inflamed lungs and that loss of CXCR3 is associated with improved survival in response to influenza virus infection in mice. In accordance with these findings, a CXCR3 antagonist resulted in a mild reduction of disease symptoms in H5N1-infected ferrets (12), and CXCR3-deficiency protected influenza-infected CCR5-deficient mice from mortality (35).

The clinical course and pathophysiological features of ARDS are marked by three phases: exudative (acute), proliferative (subacute), and fibrotic (late). Some patients with ARDS who survive the exudative phase enter a fibrotic phase that may require long-term ventilator support and/or supplementary oxygen. The alveolar edema and inflammatory exudates of earlier phases are converted to extensive alveolar duct and interstitial fibrosis. CXCL10 (32) and CXCR3 (31) have been shown to attenuate bleomycin-induced pulmonary fibrosis in mice by interruption of angiogenesis (32) and fibroproliferation (31). The data presented here and in similar studies imply that the CXCL10-CXCR3 axis may have a dual role in the acute (exudative) and chronic (fibrotic) lung processes.

Current therapeutic strategies for the acute fulminant phase of human ARDS are limited. For example, treatments for H5N1 or pandemic H1N1 infection are restricted to vaccination or early treatment with antiviral agents such as oseltamivir. Although antiviral drugs may be of benefit if administered early in the disease, neither approach is very effective in rescuing patients who have already developed ARDS. Our data indicate that not only is CXCL10 production a bystander chemokine in severe respiratory failure but also CXCL10-CXCR3 can promote development of ARDS, whether the inciting factor is of viral or nonviral origin. Thus, the CXCL10-CXCR3 axis represents an interesting therapeutic target for treatment of patients during the acute phase of ARDS.

Author disclosures are available with the text of this article at www.atsjournals.org.

Acknowledgment: The authors thank all members of our laboratories for helpful discussions.

References

1. Frutos-Vivar F, Ferguson ND, Esteban A. Epidemiology of acute lung injury and acute respiratory distress syndrome. *Semin Respir Crit Care Med* 2006;27:327–336.
2. Rubenfeld GD, Caldwell E, Peabody E, Weaver J, Martin DP, Neff M, Stern EJ, Hudson LD. Incidence and outcomes of acute lung injury. *N Engl J Med* 2005;353:1685–1693.
3. Beigel JH, Farrar J, Han AM, Hayden FG, Hyer R, de Jong MD, Lochindarat S, Nguyen TK, Nguyen TH, Tran TH, *et al*. Avian influenza a (H5N1) infection in humans. *N Engl J Med* 2005;353:1374–1385.
4. Ware LB, Matthay MA. The acute respiratory distress syndrome. *N Engl J Med* 2000;342:1334–1349.
5. Martin TR. Lung cytokines and ARDS: Roger S. Mitchell lecture. *Chest* 1999;116:2S–8S.
6. Jiang Y, Xu J, Zhou C, Wu Z, Zhong S, Liu J, Luo W, Chen T, Qin Q, Deng P. Characterization of cytokine/chemokine profiles of severe acute respiratory syndrome. *Am J Respir Crit Care Med* 2005;171:850–857.
7. Peiris JS, Yu WC, Leung CW, Cheung CY, Ng WF, Nicholls JM, Ng TK, Chan KH, Lai ST, Lim WL, *et al*. Re-emergence of fatal human influenza a subtype H5N1 disease. *Lancet* 2004;363:617–619.
8. Luster AD, Unkeless JC, Ravetch JV. Gamma-interferon transcriptionally regulates an early-response gene containing homology to platelet proteins. *Nature* 1985;315:672–676.
9. Neville LF, Mathiak G, Bagasra O. The immunobiology of interferon-gamma inducible protein 10 kD (IP-10): a novel, pleiotropic member of the C-X-C chemokine superfamily. *Cytokine Growth Factor Rev* 1997;8:207–219.
10. Moser B, Wolf M, Walz A, Loetscher P. Chemokines: multiple levels of leukocyte migration control. *Trends Immunol* 2004;25:75–84.
11. Chan MC, Cheung CY, Chui WH, Tsao SW, Nicholls JM, Chan YO, Chan RW, Long HT, Poon LL, Guan Y, *et al*. Proinflammatory cytokine responses induced by influenza a (H5N1) viruses in primary human alveolar and bronchial epithelial cells. *Respir Res* 2005;6:135.
12. Cameron CM, Cameron MJ, Bermejo-Martin JF, Ran L, Xu L, Turner PV, Ran R, Danesh A, Fang Y, Chan PK, *et al*. Gene expression analysis of host innate immune responses during lethal H5N1 infection in ferrets. *J Virol* 2008;82:11308–11317.
13. Chan MC, Chan RW, Yu WC, Ho CC, Chui WH, Lo CK, Yuen KM, Guan YI, Nicholls JM, Peiris JS. Influenza h5n1 virus infection of polarized human alveolar epithelial cells and lung microvascular endothelial cells. *Respir Res* 2009;10:102.
14. Korpi-Steiner NL, Bates ME, Lee WM, Hall DJ, Bertics PJ. Human rhinovirus induces robust IP-10 release by monocytic cells, which is independent of viral replication but linked to type i interferon receptor ligation and STAT1 activation. *J Leukoc Biol* 2006;80:1364–1374.
15. Abdullah F, Ovadia P, Feuerstein G, Neville LF, Morrison R, Mathiak G, Whiteford M, Rabinovici R. The novel chemokine mob-1: involvement in adult respiratory distress syndrome. *Surgery* 1997;122:303–312.
16. Neville LF, Abdullah F, McDonnell PM, Young PR, Feuerstein GZ, Rabinovici R. Mob-1 expression in IL-2-induced ARDS: regulation by TNF-alpha. *Am J Physiol* 1995;269:L884–L890.
17. Rossi D, Zlotnik A. The biology of chemokines and their receptors. *Annu Rev Immunol* 2000;18:217–242.
18. Szretter KJ, Gangappa S, Belser JA, Zeng H, Chen H, Matsuoka Y, Sambhara S, Swayne DE, Tumpey TM, Katz JM. Early control of H5N1 influenza virus replication by the type I interferon response in mice. *J Virol* 2009;83:5825–5834.
19. Frieman MB, Chen J, Morrison TE, Whitmore A, Funkhouser W, Ward JM, Lamirande EW, Roberts A, Heise M, Subbarao K, *et al*. SARS-CoV pathogenesis is regulated by a STAT1 dependent but a type I, II and III interferon receptor independent mechanism. *PLoS Pathog* 2010;6:e1000849.
20. Goggel R, Winoto-Morbach S, Vielhaber G, Imai Y, Lindner K, Brade L, Brade H, Ehlers S, Slutsky AS, Schutze S, *et al*. PAF-mediated pulmonary edema: a new role for acid sphingomyelinase and ceramide. *Nat Med* 2004;10:155–160.
21. Gentleman RC, Carey VJ, Bates DM, Bolstad B, Dettling M, Dudoit S, Ellis B, Gautier L, Ge Y, Gentry J, *et al*. Bioconductor: open software development for computational biology and bioinformatics. *Genome Biol* 2004;5:R80.
22. Imai Y, Kuba K, Neely GG, Yaghubian-Malhami R, Perkmann T, van Loo G, Ermolaeva M, Veldhuizen R, Leung YH, Wang H, *et al*. Identification of oxidative stress and toll-like receptor 4 signaling as a key pathway of acute lung injury. *Cell* 2008;133:235–249.

23. Sly PD, Collins RA, Thamrin C, Turner DJ, Hantos Z. Volume dependence of airway and tissue impedances in mice. *J Appl Physiol* 2003;94:1460–1466.
24. Arnhold J, Flemmig J. Human myeloperoxidase in innate and acquired immunity. *Arch Biochem Biophys* 2010;500:92–106.
25. Cassatella MA, Gasperini S, Calzetti F, Bertagnin A, Luster AD, McDonald PP. Regulated production of the interferon-gamma-inducible protein-10 (IP-10) chemokine by human neutrophils. *Eur J Immunol* 1997;27:111–115.
26. Hartl D, Krauss-Etschmann S, Koller B, Hordijk PL, Kuijpers TW, Hoffmann F, Hector A, Eber E, Marcos V, Bittmann I, *et al*. Infiltrated neutrophils acquire novel chemokine receptor expression and chemokine responsiveness in chronic inflammatory lung diseases. *J Immunol* 2008;181:8053–8067.
27. Sorensen TL. Targeting the chemokine receptor CXCR3 and its ligand CXCL10 in the central nervous system: potential therapy for inflammatory demyelinating disease? *Curr Neurovasc Res* 2004;1:183–190.
28. Medoff BD, Sauty A, Tager AM, Maclean JA, Smith RN, Mathew A, Dufour JH, Luster AD. IFN-gamma-inducible protein 10 (CXCL10) contributes to airway hyperreactivity and airway inflammation in a mouse model of asthma. *J Immunol* 2002;168:5278–5286.
29. Hancock WW, Gao W, Csizmadia V, Faia KL, Shemmeri N, Luster AD. Donor-derived IP-10 initiates development of acute allograft rejection. *J Exp Med* 2001;193:975–980.
30. Tager AM, Kradin RL, LaCamera P, Bercury SD, Campanella GS, Leary CP, Polosukhin V, Zhao LH, Sakamoto H, Blackwell TS, *et al*. Inhibition of pulmonary fibrosis by the chemokine IP-10/CXCL10 regulation of pulmonary fibrosis by chemokine receptor CXCR3. *Am J Respir Cell Mol Biol* 2004;31:395–404.
31. Jiang D, Liang J, Hodge J, Lu B, Zhu Z, Yu S, Fan J, Gao Y, Yin Z, Homer R, *et al*. Regulation of pulmonary fibrosis by chemokine receptor CXCR3. *J Clin Invest* 2004;114:291–299.
32. Keane MP, Belperio JA, Arenberg DA, Burdick MD, Xu ZJ, Xue YY, Strieter RM. IFN-gamma-inducible protein-10 attenuates bleomycin-induced pulmonary fibrosis via inhibition of angiogenesis. *J Immunol* 1999;163:5686–5692.
33. Takeuchi O, Akira S. Pattern recognition receptors and inflammation. *Cell* 2012;140:805–820.
34. Barrenschee M, Lex D, Uhlig S. Effects of the TLR2 agonists MALP-2 and Pam3Cys in isolated mouse lungs. *PLoS ONE* 2012;5:e13889.
35. Fadel SA, Bromley SK, Medoff BD, Luster AD. CXCR3-deficiency protects influenza-infected CCR5-deficient mice from mortality. *Eur J Immunol* 2008;38:3376–3387.
36. Dufour JH, Dziejman M, Liu MT, Leung JH, Lane TE, Luster AD. IFN-gamma-inducible protein 10 (IP-10; CXCL10)-deficient mice reveal a role for IP-10 in effector T cell generation and trafficking. *J Immunol* 2002;168:3195–3204.
37. Hancock WW, Lu B, Gao W, Csizmadia V, Faia K, King JA, Smiley ST, Ling M, Gerard NP, Gerard C. Requirement of the chemokine receptor CXCR3 for acute allograft rejection. *J Exp Med* 2000;192:1515–1520.
38. Yamamoto M, Sato S, Hemmi H, Hoshino K, Kaisho T, Sanjo H, Takeuchi O, Sugiyama M, Okabe M, Takeda K, *et al*. Role of adaptor TRIF in the MyD88-independent toll-like receptor signaling pathway. *Science* 2003;301:640–643.
39. Imai Y, Kuba K, Rao S, Huan Y, Guo F, Guan B, Yang P, Sarao R, Wada T, Leong-Poi H, *et al*. Angiotensin-converting enzyme 2 protects from severe acute lung failure. *Nature* 2005;436:112–116.
40. Daidoji T, Koma T, Du A, Yang CS, Ueda M, Ikuta K, Nakaya T. H5N1 avian influenza virus induces apoptotic cell death in mammalian airway epithelial cells. *J Virol* 2008;82:11294–11307.
41. Du A, Daidoji T, Koma T, Ibrahim MS, Nakamura S, de Silva UC, Ueda M, Yang CS, Yasunaga T, Ikuta K, *et al.* Detection of circulating asian H5N1 viruses by a newly established monoclonal antibody. *Biochem Biophys Res Commun* 2009;378:197–202.
42. Smyth GK. Linear models and empirical bayes methods for assessing differential expression in microarray experiments. *Stat Appl Genet Mol Biol* 2004;3:3.